Importance of small-scale anisotropy in the turbulent/nonturbulent interface region of turbulent free shear flows

O. R. H. Buxton, M. Breda, and K. Dhall
Department of Aeronautics, Imperial College London, London SW7 2AZ, United Kingdom

(Received 27 July 2018; published 18 March 2019)

There has been much debate over the past decade or so over the scaling of the thickness of the turbulent/nonturbulent (TNT) interface for turbulent shear flows. It is generally considered to consist of the outer viscous superlayer, in which viscous processes are significant, and an inner turbulent sublayer which is dominated by inertial processes. Various authors have stated that the interface thickness scales with the Taylor length scale λ while others state that it scales with the Kolmogorov length scale η [Buxton *et al.*, Phys. Fluids **23**, 061704 (2011)]. Frequently, only self-similar turbulent flows are considered in which a single value of either λ or η is sufficient to scale various phenomena, including the thickness of the TNT interface. In this paper we show that for flows which are not self-similar the local Kolmogorov length scale increases quite significantly as one moves closer to the boundary between the turbulent and nonturbulent fluid. We find that the variation of this local Kolmogorov length scale with normal distance from the TNT boundary may be collapsed by the local Kolmogorov length scale computed from the TNT boundary itself. We subsequently show that this variation in local Kolmogorov length scale occurs concurrently with an increase in the small-scale anisotropy in the TNT interface. This anisotropy peaks at the boundary between the viscous superlayer and the turbulent sublayer, suggesting that these two sublayers are in fact quite distinct from one another. We show that these results hold for a number of different TNT interfaces from various flows and with the bulk turbulence being in a variety of states of development. The local viscous scaling that we obtain, along with an increase in anisotropy primarily driven by an increased magnitude of velocity gradients in the TNT-boundary-normal direction, leads us to draw an analogy between TNT interfaces and the wall in wall-bounded turbulence.

DOI: 10.1103/PhysRevFluids.4.034603

I. INTRODUCTION

Fascinatingly, the turbulent and nonturbulent regions of free shear flows are demarcated with a sharp and beautifully defined interface such that the fluid transitions from nonturbulent to turbulent (and vice versa) over a very short distance. This turbulent/nonturbulent (TNT) interface is typically highly contorted and may be characterized by a fractal dimension [1,2]. These contortions are caused by the hierarchy of turbulent eddies within the turbulent portion of the fluid wrinkling the interface itself. The interface is important since significant transfers of mass, momentum, vorticity, energy, and scalar (if present) occur across the TNT interface. In particular, the entrainment rate is dictated by the dynamics of the flow in the vicinity of the interface, which in turn sets the spreading rate of a turbulent shear flow (along with the spatial decay of the mean momentum or momentum deficit for a free shear flow) [3].

The seminal work of Corrsin and Kistler [4] was the first to hypothesise the nature of the boundary between turbulent and nonturbulent fluid. They noted that nonturbulent fluid is irrotational, whereas turbulent fluid is not, i.e., $\omega_i\omega_i = \omega^2 > 0$, and hence the TNT boundary is simply an enstrophy ($\omega^2 = 0$) surface. Given that the inertial source term of the vorticity transport equation

 ©2019 American Physical Society

is necessarily zero along this surface, the only means by which vorticity can be transferred from turbulent to nonturbulent fluid is through the direct action of molecular viscosity. Due to its viscous nature, they termed this layer the viscous superlayer and provided an explanation for why the TNT interface is thin. The existence of this viscous superlayer has subsequently been experimentally confirmed by Holzner and Lüthi [5] and characterized by Taveira and da Silva [6], who suggested that its thickness scaled with the Kolmogorov length scale $\eta = (\nu^3/\varepsilon)^{1/4}$, where ν is the kinematic viscosity of the fluid and ε is the dissipation rate of turbulent kinetic energy. This is the scaling factor for Kolmogorov's first similarity hypothesis and embodies the length scale at which viscosity acts to dissipate turbulent kinetic energy in a turbulent flow, i.e., it is representative of the smallest scales present within the flow. Note that Corrsin and Kistler [4] postulated that the viscous superlayer thickness may scale with η, but their intuition only led them to say that it should scale with some viscous length scale.

In contrast to the viscous superlayer, the TNT interface itself is actually a layer of finite thickness in which the statistical characteristics of the turbulence adapt to those of the bulk flow. It has thus been educed that the TNT interface consists of both the viscous superlayer and a turbulent sublayer (buffer layer) in which inertial processes take precedence over viscous effects, while the turbulence properties adjust to those of the bulk flow [7,8]. Much work has subsequently concentrated on trying to find the correct scaling for the thickness of the TNT interface. This has largely focused on examining one-point statistics, usually the enstrophy ω^2, conditioned on distance away from a fixed position in the TNT interface, often the TNT boundary. Bisset *et al.* [9] were the first to do this, defining the TNT boundary using a small but nonzero threshold of vorticity (to account for background numerical noise) from the flat-plate-wake simulation data they used. They showed that the vorticity jump occurred over a length scale $\delta_\omega \sim \lambda$, where λ is the Taylor length scale. This is a mixed length scale defined in terms of the turbulent kinetic energy (large scale) and the dissipation rate (fine scale) which is typically representative of inertial range fluctuations in a turbulent flow. This $\delta_\omega \sim \lambda$ scaling has subsequently been shown to hold not only for wakes, but for axisymmetric jets [10], planar jets [7], mixing layers [11], and boundary layers [12].

More recently, some doubt has been thrown over this $\delta_\omega \sim \lambda$ scaling. It can be shown that the ratio $\lambda/\eta \sim \mathrm{Re}_\lambda^{1/2}$, where Re_λ is a local turbulent Reynolds number based on the local rms velocity fluctuation and Taylor length scale. Silva *et al.* [13] used the fact that $\delta_\omega/\lambda \sim \mathrm{Re}_\lambda^{-1/2}$ concomitantly with $\eta/\lambda \sim \mathrm{Re}_\lambda^{-1/2}$ to argue that in fact the interface thickness scales with the Kolmogorov length scale rather than the Taylor length scale. As they point out, the previously cited works were conducted for modest Reynolds numbers at which it is very difficult to distinguish between $O(10)\eta$ and λ. In fact, they conclude that for higher-Reynolds-number flows ($\mathrm{Re}_\lambda \gtrsim 200$), the overall thickness of the TNT interface is $\delta_\omega \approx 17\eta$, with the viscous superlayer being of thickness approximately equal to 5η and the turbulent sublayer being of thickness approximately equal to 12η. These results are complementary to those achieved by Watanabe *et al.* [14–16], who have shown that the ratio δ_ω/λ decreases as the Reynolds number increases, casting doubt on the $\delta_\omega \sim \lambda$ scaling. Since many industrial and environmental flows occur at very large Reynolds numbers, it is clearly imperative to get the correct scaling for the TNT interface from a modeling perspective. Regardless of whether the interface scales with λ, η, or indeed some other viscous length scale ℓ, these are all local scales that must be computed at a given spatial location.

Free shear flows are inhomogeneous, which therefore raises the question of which spatial location should be chosen to compute $\{\eta, \lambda, \ell\}$. More often than not this detail is omitted from the literature such that we do not know whether, for example, the centerline Taylor scale is used or the bulk average Taylor scale from the turbulent portion of the flow. Much of the existing literature (e.g., [7,11,13]) has considered the self-similar regions of turbulent flows. In the strictest sense, self-similarity requires that all of the statistical profiles, e.g., mean velocity, turbulent kinetic energy (TKE), dissipation rate, etc., at particular spatial locations of these flows can be collapsed with a simple normalization. Specifically, the cross-stream coordinate (usually y) is normalized with a single flow-specific macroscopic length scale (e.g., the vorticity thickness of a mixing layer) and

the statistical quantity of interest is normalized with a single value, usually the centerline value, i.e., normalization of the TKE profile with the TKE at the centerline of the flow. Self-similarity thus has two consequences relevant to the scaling of the TNT interface. First, by virtue of the fact that the statistical profiles are normalized with a macroscopic (large-scale) length scale, the variation of, e.g., dissipation or TKE (and hence η and λ) ought to be small over a length scale $\delta_\omega \sim \lambda$. Second, a single value of either η or λ is sufficient to scale the flow at a given streamwise location, even if the flow itself is inhomogeneous. However, for non-self-similar flows it is not clear *a priori* from which spatial location one should choose to compute η or λ, which may vary considerably due to the flow's inhomogeneity. It should be noted that frequently some aspects of turbulent flows achieve a state of self-similarity, usually the mean velocity profile does so at the farthest upstream location, without becoming fully self-similar. In particular, Breda and Buxton [17] showed that the profile of mean dissipation rate, a key constituent of the Kolmogorov length scale, did not achieve a self-similar state at a downstream location at which both the mean velocity and Reynolds stress profiles had become self-similar in axisymmetric jets.

In this paper we draw a (loose) analogy between the TNT interface and the wall for wall-bounded turbulence. Such an analogy may have been previously inferred from the nomenclature of "buffer layer" used by van Reeuwijk and Holzner [8] to describe the turbulent sublayer. Near-wall turbulence consists of a thin layer very close to the wall in which viscous processes are dominant followed by a slightly thicker buffer layer in which inertial processes gradually usurp the viscous ones in importance before the bulk turbulence is reached in the logarithmic layer. The turbulence properties of wall-bounded turbulence are collapsed with a local length scale that depends on the shear stress at the wall, not within the turbulent bulk region of the flow. Further, one of the most important effects that the wall has on the near-wall turbulence is to introduce a substantial anisotropy, with gradients in the wall-normal direction becoming large in comparison to gradients in the wall-parallel directions. In this paper we will consider two different data sets, one numerical and one experimental, and examine the small-scale anisotropy in the TNT interface region of free shear flows with differing flow properties.

II. DATA SETS

Two data sets are considered in Sec. III of this paper, one experimental and one from direct numerical simulation (DNS). The vast majority of the results presented will be from the DNS data set with comparison drawn against the experimental data set simply to broaden the scope of the conclusions. The DNS is of a planar mixing layer and the experimental data are from a series of turbulent jets at various stages of development, which broadens the scope of the conclusions since there are multiple types of TNT interfaces present in such flows, with different properties.

A. DNS mixing layer data

The first data set that we consider is from the far field of a turbulent planar mixing layer DNS, first published in Ref. [18]. Mixing layers produce two different types of TNT interfaces. In one interface, termed the high-speed interface, the nonturbulent fluid is advecting faster than the turbulent fluid and in the other, the low-speed interface, the turbulent fluid is advecting more rapidly than the nonturbulent fluid. The flow is a planar mixing layer formed from two uniform streams of velocities U_1 and U_2, in the ratio $U_1/U_2 = 2$, either side of a splitter plate of thickness h, similar to the study of Laizet *et al.* [19]. The computational domain ($L_x \times L_y \times L_z = 230.4h \times 48h \times 28.8h$) is discretized onto a Cartesian mesh that is stretched in the cross-stream (y) direction. This mesh consists of $2049 \times 513 \times 256$ mesh nodes, although in this paper we will only consider a subdomain consisting of the final $301 \times 513 \times 256$ in which the turbulence is fully developed with self-similar mean velocity profiles throughout, similar to the one considered in Ref. [20], although the profiles of higher-order statistics are not self-similar. The results are extracted from three statistically independent snapshots which were stored and analyzed. Since this domain is small in streamwise

extent, we make the assumption that the turbulence properties are homogeneous in x within this subdomain, enabling us to better converge our statistics as only a limited number of snapshots were available. This includes the threshold value that we choose to define the position of the turbulence boundary which remains a constant across the streamwise extent of this subdomain. Due to the spanwise periodic boundary conditions, we also assume that the flow is homogeneous in the z direction. Note that these assumptions were also adopted in Refs. [20,21]. The mesh is stretched in the cross-stream (y) direction, which leads to a minimal mesh size of $\Delta y \approx 0.03h$, while it is of a constant size in the streamwise and spanwise directions of $\Delta x = \Delta z = 0.1125h$, which corresponds to approximately $2.5\eta_{\mathrm{cl}}$, where η_{cl} is the Kolmogorov length scale computed along the centerline. The time step $\Delta t = 0.05h/U_c$, where $U_c = (U_1 + U_2)/2$, is low enough to satisfy the Courant-Friedrichs-Lewy condition, ensuring temporal stability of the solution. The Reynolds number based on U_c and h (Re_h) is 1000 and the Taylor Reynolds number along the centerline of the sub domain, computed as $\mathrm{Re}_\lambda = u'\lambda/\nu$, is approximately equal to 200.

The code INCOMPACT3D [22], based on sixth-order compact schemes for spatial discretization and second-order Adams-Bashforth schemes for time advancement, is used to solve the incompressible nondimensionalized Navier-Stokes equations. The length and velocity scales used for the nondimensionalization are h and U_c, respectively. To treat the incompressibility condition, a projection method is used requiring the solution of a Poisson equation for the pressure. This equation is fully solved in spectral space via the use of the relevant three-dimensional fast Fourier transforms. The boundary conditions are inflow and outflow in the streamwise direction (velocity boundary conditions of the Dirichlet type), free slip in the cross-stream direction at $y = 0, L_y$, and periodic in the spanwise direction. The pressure mesh is staggered from the velocity mesh to avoid spurious pressure oscillations. More details on the simulation, in particular the generation of the inlet or initial conditions (including the boundary layers on both sides of the splitter plate), can be found in Ref. [19] and more details about the code, its validation, and the original treatment of the pressure in spectral space can be found in Ref. [22]. All velocity gradients were subsequently computed during the postprocessing using a sixth-order-accurate Lagrange interpolating polynomials scheme.

B. Tomographic particle image velocimetry turbulent jet data

The jet data that are used are from the same data set described in Ref. [23] in which experiments were conducted in an axisymmetric jet facility. Two orifices of identical open area (D^2) were attached to the jet exit and the flow rate was controlled to ensure that the Reynolds number $\mathrm{Re}_D = UD/\nu = 1 \times 10^4$, in which U is the volumetric flow rate divided by the open exit area, was kept constant across both jets. One was a simple round orifice while the other was a repeating fractal pattern of fractal dimension 1.5, first described in Ref. [24], and with three fractal iterations. This fractal orifice was shown to break down the azimuthally coherent structures present in the near field of the jet such that a direct comparison between jets with and without coherent structures present could be made [17,23]. The Taylor Reynolds number, defined as $\mathrm{Re}_\lambda = u'\lambda/\nu$, was computed from the turbulent bulk of the flow, i.e., that which exceeded our enstrophy threshold. Re_λ ranged from approximately 450 at $x/D = 2$ for the round jet to $\mathrm{Re}_\lambda \approx 220$ at $x/D = 25$ for both jets. There was a substantially smaller value of $\mathrm{Re}_\lambda \approx 225$ for the fractal jet at $x/D = 2$ and intermediate values of $\mathrm{Re}_\lambda \approx 330$ (350) for the fractal (round) jets at $x/D = 10$.

Three-dimensional three-component velocity data were produced through tomographic particle image velocimetry (PIV) experiments [25] in three slices of the jet parallel to the r-θ plane, of thickness $0.33D$. Note that the data are presented in a cylindrical polar coordinate system (x, r, θ) in which x is the streamwise direction, r is the radial direction, and θ is the azimuthal direction. These slices were centered on the streamwise locations $x/D = 2$, 10, and 25. A clearly defined annular shear layer surrounding a potential core was present for both the round and fractal jets at $x/D = 2$, giving us access to both an inner TNT interface (between the potential core and the shear layer) and an outer TNT interface (between the shear layer and the background fluid). The azimuthal coherent structures were significantly suppressed in the shear layer of the fractal jet,

whereas they were highly energetic for the round jet [17]. Only the outer TNT interface existed at $X/D = 10, 25$ with the mean velocity and Reynolds stress profiles (but not the dissipation-rate profile) being self-similar at $x/D = 25$ but not at $x/D = 10$. At each measurement station 1500 images were acquired at a sufficiently low acquisition frequency that adjacent velocity snapshots in the sequence were statistically independent of one another using four cameras in forward scatter.

The PIV images were processed using the MART algorithm (six iterations), a multiplicative algebraic reconstruction [26]. To improve the quality of the reconstruction, the dark background previously acquired was subtracted. Sliding minimum subtraction, Gaussian smoothing using a 3×3 pixel kernel (to reduce the background noise), and sharpening (to reduce the number of ghost particles) were also performed on the raw images, allowing the particle diameter to be of the order of two pixels and the particle density to be within 0.04 and 0.05 particles per pixel. Volume self-calibration [27] was then applied to the reconstructed particle image volumes to improve accuracy. The vectors were reconstructed in three steps: an initial recursive direct correlation, followed by two iterations of motion tracking enhancement [28] to reduce the number of ghost particles and a final recursive direct correlation. The final interrogation volumes were of size $48 \times 48 \times 48$ voxels, with a 75% overlap between adjacent interrogation volumes, which led to a spatial resolution of between 5η and 11η.

To correct the nonzero divergence introduced through experimental noise, the data were corrected using the divergence correction scheme of Ref. [29]. This scheme is based on a nonlinear optimization-based constraint which minimally alters the acquired velocity field while restricting the magnitude of the divergence to a maximum tolerance. The objective function to be minimized is the ensemble average of the turbulent kinetic energy $\tilde{k}$ added to the measured velocity field to ensure that the divergence is kept below the tolerance threshold chosen. In this case the divergence error was set to be $|\partial u_i/\partial x_i| < 10\ \mathrm{s}^{-1}$, which led to an average $\tilde{k}/U_{\mathrm{cl}} < 5\%$, where U_{cl} is the centerline velocity of the jet. All velocity gradients were computed using a fourth-order-accurate central differencing scheme. More details on the experimental setup can be found in Ref. [17], with a more detailed discussion of the acquisition and processing of the tomographic PIV data found in Ref. [23].

III. RESULTS

A. TNT interface detection

Due to the presence of numerical noise, it is necessary to set a nonzero threshold of enstrophy in order to detect the TNT interface (see, e.g., [7,9]). The most robust way to set this threshold is to compute the overall proportion of a given data set identified as turbulent, i.e., $\omega^2 > \omega^2_{\mathrm{thresh}}$, where $\omega^2_{\mathrm{thresh}}$ is the enstrophy threshold chosen, as a function of $\omega^2_{\mathrm{thresh}}$ [3]. If a plateau region can be found in which the percentage of fluid identified as being turbulent remains roughly invariant to small changes in $\omega^2_{\mathrm{thresh}}$, then a robust threshold has been identified. Such a plot for the DNS data is presented in Fig. 1(a), which shows that a plateau can be identified and we chose to set our threshold (marked with the dashed line) at $\omega^2_{\mathrm{thresh}}/\langle\omega^2\rangle(t) = 0.025$. This threshold is a function of the local bulk average of the enstrophy for each time step to account for variation between time steps. Note that this is the identical threshold to that used in Ref. [20] to distinguish between turbulent and nonturbulent fluid, however the plateau region is not completely flat. For this reason, a sensitivity study was conducted to ensure that the results presented later on were insensitive to small changes in the threshold chosen which was indeed found to be the case. Figure 1(b) presents an illustrative example of both the high-speed and low-speed interfaces detected in a particular x-y plane for a particular time step. Note that we exclude both islands of turbulent flow in the nonturbulent region that have become separated from the turbulent bulk (usually such islands remain connected to the turbulent bulk when considering the three-dimensional topography) and holes of irrotational fluid in the turbulent region from the conditional statistics presented subsequently. The interface detection algorithm will naturally produce some x locations at which the TNT interface has more than one y location due to contortions of the interface that lead to overhangs. Such overhangs can be visualized

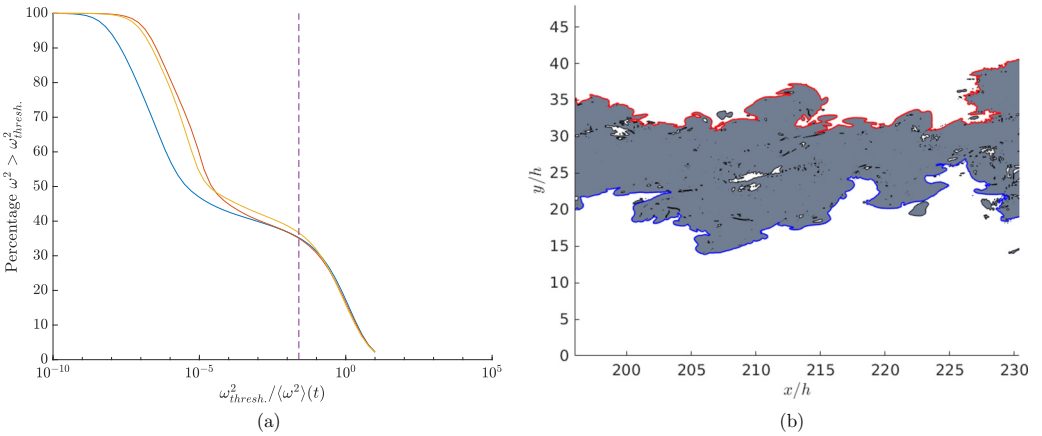

FIG. 1. DNS data set. (a) Percentage of data points identified as being turbulent as a function of enstrophy threshold for all three time steps considered. The chosen threshold is denoted by the dashed line. (b) Example of the turbulent region defined according to the chosen threshold. The red line denotes the high-speed TNT interface and the blue line denotes the low-speed TNT interface.

in Fig. 1(b) and are discussed at some length in Ref. [30]. Note that when producing our conditional statistics, special treatment is required for these overhangs. Cases in which a traverse along the interface normal direction y^* (see Sec. III B) crosses the TNT interface on more than one occasion are excluded from our conditional statistics. Precisely this scenario is caused by the existence of overhangs. The exclusion of these traverses that cross the TNT interface more than once is in keeping with similar methodology used previously (e.g., [31]).

B. Coordinate transformation

As mentioned in Sec. I in this paper, we draw an analogy between the TNT interface and a wall. Unlike a wall, however, the interface is highly contorted, thereby requiring a coordinate system transform in order to draw the analogy. This is illustrated in Fig. 2, which shows how the interface (defined in the present work in only two dimensions since the third dimension is not needed in the present analysis) can be mapped onto a new coordinate system (x^*, y^*), which we will refer to as the interface coordinate system. In this case x^* is a coordinate tangential to the interface and y^* is a coordinate normal to the interface with the interface location being defined as $y^* = 0$ with the turbulent portion being subsequently defined as $y^* > 0$. Both the tangent and normal lines defining the directions of x^* and y^*, respectively, are defined in two dimensions only. The velocity vector, and subsequently velocity fluctuations and gradients, may now also be defined in the interface coordinate system such that $\boldsymbol{u} = (u_{x^*}, u_{y^*}, u_z)^T$. This yields velocity components, discussed further in Sec. III E,

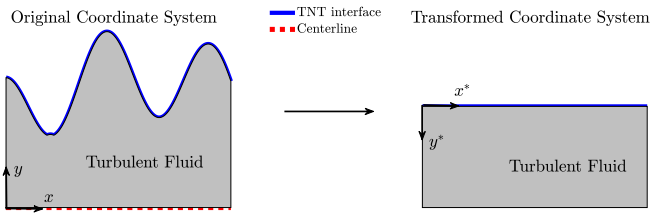

FIG. 2. Illustration of the coordinate transform from the Cartesian set (x, y) to the TNT interface parallel or normal set (x^*, y^*).

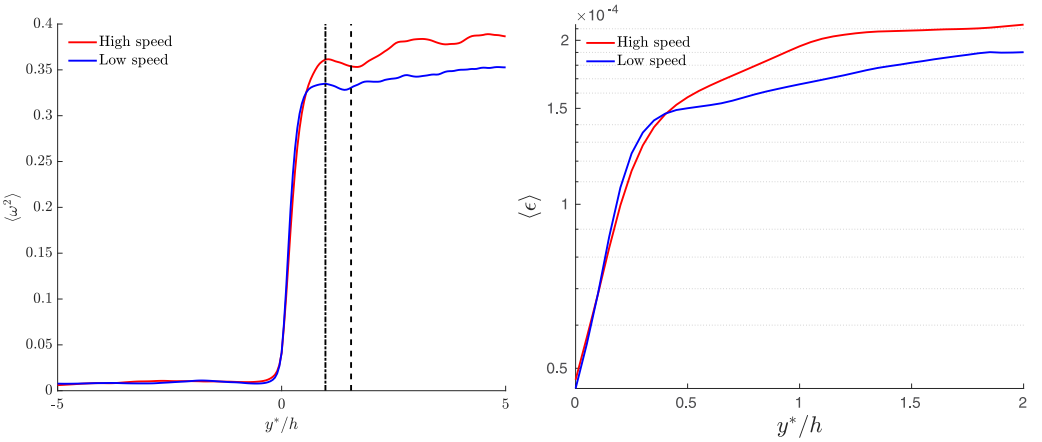

FIG. 3. Conditional (a) mean enstrophy $\langle\omega^2\rangle$ and (b) dissipation rate ε as a function of interface-normal distance y^* for both interfaces of the mixing layer. The dashed black line in (a) indicates the Taylor length scale as computed from the centerline of the flow and the dash-dotted black line indicates a thickness of 17η, where η is the Kolmogorov length scale computed along the centerline.

that are parallel (u_{x^*}) and normal (u_{y^*}) to the interface (locally) in the x-y plane in addition to the standard (Cartesian) spanwise component of velocity (u_z).

C. Conditional mean statistics in the TNT interface region

The conditional mean enstrophy $\langle\omega^2\rangle$ as a function of y^* is presented in Fig. 3. The form of $\langle\omega^2\rangle(y^*)$ observed is similar to those presented in, e.g., [3,9], suggesting that $\delta_\omega \approx 1.5h$. Note that in this paper we do not wish to comment on the correct scaling for the TNT interface thickness δ_ω since we do not have access to data over a sufficiently broad range of Reynolds numbers, and this has been discussed at length recently in Ref. [13]. For this reason we choose to use the (uncontroversial) h, i.e., the length scale input to the DNS solver, as the normalizing length scale for y^* but note that the centerline Taylor length scale is $\lambda \approx 1.55h$. This length scale has been marked on the figure with a dashed black line. In addition, we have marked a distance of 17η, the TNT interface thickness quoted in Ref. [13], with a dash-dotted black line. It is thus clear that the enstrophy jump occurs over a distance that is approximately equal in size to the Taylor length scale (or 17 Kolmogorov length scales), which is consistent with previously reported literature (e.g., [7,10–13]). This gives us confidence in the interface detection approach described in Sec. III A.

Figure 3(b) shows the conditional mean dissipation rate $\langle\varepsilon\rangle = 2\nu\langle s_{ij}s_{ij}\rangle$, in which s_{ij} is the rate-of-strain tensor (the symmetric part of $a_{ij} = \partial u_i/\partial x_j$), as a function of y^*. The $\langle\varepsilon\rangle$ axis is logarithmic, meaning that the apparently linear increase of $\langle\varepsilon\rangle$ with y^* suggests that there is an exponential increase in the dissipation rate moving from the turbulence boundary through the presumed viscous superlayer (i.e., that part of the TNT interface closest to the turbulence boundary). This is a similar finding for the rate of increase of conditionally averaged enstrophy through the viscous superlayer as presented in [8]. In that case it was shown that the Kolmogorov length scale adequately collapsed the variation of conditionally averaged enstrophy with interface-normal distance in their temporal planar jets. While we do not have sufficient data sets at different Reynolds numbers to confidently state that the Kolmogorov length scale also collapses the exponential increase of $\langle\varepsilon\rangle$ with y^*, we note the collapse between the high-speed and low-speed interfaces.

The enstrophy transport equation is given by

$$\frac{1}{2}\left(\frac{\partial\omega^2}{\partial t} + u_j\frac{\partial\omega^2}{\partial x_j}\right) = \omega_i s_{ij}\omega_j + \nu\frac{\partial^2}{\partial x_j\partial x_j}\left(\frac{\omega^2}{2}\right) - \nu\frac{\partial\omega_i}{\partial x_j}\frac{\partial\omega_i}{\partial x_j}, \tag{1}$$

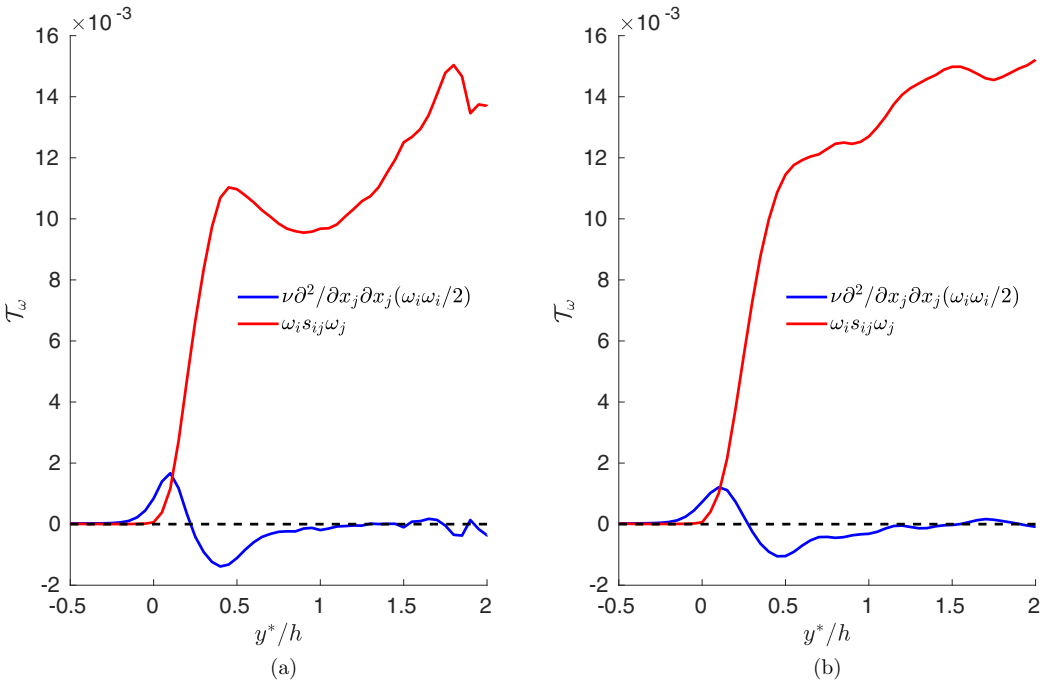

FIG. 4. Conditional mean value for the terms $\mathcal{T}_\omega$ of the enstrophy transport equation as a function of interface-normal distance y^* for both (a) the low-speed interface and (b) the high-speed interface of the mixing layer.

in which s_{ij} is the strain-rate tensor

$$s_{ij} = \frac{1}{2}\left(\frac{\partial u_i}{\partial x_j} + \frac{\partial u_j}{\partial x_i}\right). \tag{2}$$

Let us generically call the source and sink terms on the right-hand side of (1) $\mathcal{T}_\omega$, which are, from left to right, the vortex stretching term, the viscous diffusion term, and the viscous dissipation term. The vortex stretching term $\mathcal{P}_\omega = \omega_i s_{ij}\omega_j$ is the inertial mechanism by which enstrophy is amplified or suppressed due to the interaction between strain rate and rotation in the flow and $\langle\omega_i s_{ij}\omega_j\rangle > 0$ is a key indicator for developed turbulent flow [32]. On the other hand, $\mathcal{D}_\omega = \nu\partial^2/\partial x_j\partial x_j(\omega^2/2)$ is the viscous diffusion term. Clearly along an isosurface of $\omega^2 = 0$ this is the only nonzero source term thereby yielding the original intuition of Corrsin and Kistler [4] regarding the viscous superlayer.

Figure 4 shows the variation of $\mathcal{T}_\omega$ with y^* for both the low-speed and high-speed interfaces. The variation of both $\mathcal{P}_\omega$ and $\mathcal{D}_\omega$ with y^* is extremely similar to that presented for the TNT interface of planar turbulent jets in Ref. [6]. Note that there is a small but nonzero contribution to the viscous diffusion term beyond the turbulence boundary. This result is consistent with the finding of Taveira and da Silva [6]. Evidently there must be a source of enstrophy in the nonturbulent fluid in order for the turbulent portion to grow in time and space. This is also consistent with the finding of da Silva and Pereira [33], who observed non-negligible viscous dissipation of turbulent kinetic energy in the nonturbulent fluid adjacent to the turbulence boundary. This was attributed to instantaneous pure shear motions induced by the large-sale entraining motions in the nonturbulent fluid and highlights the fact that viscous processes are indeed significant on both sides of the turbulence boundary. The enstrophy amplification term $\mathcal{P}_\omega$ continues to increase beyond the TNT interface region, into the turbulent bulk, which is also consistent with the results of Taveira and da Silva [6]. Note that

$\mathcal{P}_\omega = 0$ at $y^* = 0$, which is the original intuition of Corrsin and Kistler [4], giving us confidence in our interface detection threshold.

In Ref. [6] the viscous superlayer is arbitrarily defined as being the spatial region for which the ratio $|\mathcal{D}_\omega/\mathcal{P}_\omega| > 2$. Contrastingly, in Ref. [8] the viscous superlayer is defined in terms of the contribution towards the total entrainment velocity having a negligible contribution from the $\mathcal{P}_\omega$ term (less than 5% in that paper). In both cases the extent of the viscous superlayer is perhaps counterintuitively defined in terms of the relative contribution of the inertial term. Instead we will focus on the viscous diffusion term $\mathcal{D}_\omega$, which we clearly expect to act as a source of enstrophy in the viscous superlayer. We note, similarly to Taveira and da Silva [6], that $\mathcal{D}_\omega$ is an increasing function of y^* close to the turbulent boundary before reaching a local maximum, then a local minimum, and then finally settling to $\mathcal{D}_\omega \approx 0$ (as expected) in the turbulent bulk portion of the flow. We may thus set a more robust definition of the viscous superlayer by defining its extent as the location at which the diffusion term first crosses zero, thereby demarcating regions of the flow in which the diffusion term acts as a source as opposed to a sink of enstrophy (or indeed becomes negligible). It should be noted that occurs at $y^*/h \approx 0.28 \approx 5\eta_{\mathrm{cl}}$ for both interfaces. Note that this is the same thickness quoted in Ref. [13] for the thickness of the viscous superlayer.

D. Local turbulent length scales in the TNT interface region

The Kolmogorov length scale is as defined as

$$\frac{\eta}{h} = \left(\frac{1}{2\,\mathrm{Re}_h^2\langle\tilde{s}_{ij}\tilde{s}_{ij}\rangle}\right)^{1/4}, \tag{3}$$

where $\tilde{s}_{ij}$ is the nondimensional rate-of-strain tensor. Note that ensemble averaging is performed when computing the mean strain-rate magnitude. It is frequently not reported what constitutes this ensemble when reporting on the scaling of δ_ω, the TNT interface thickness, in the literature. Let us define a bulk Kolmogorov length scale $\langle\eta\rangle$ as being the solution to (3) in which the ensemble constitutes all fluid defined as being turbulent, i.e., that for which $\omega^2 > \omega^2_{\mathrm{thresh}}$. Now let us define the local Kolmogorov length scale η_l: η_l is computed as the conditionally averaged value of the Kolmogorov length scale, computed as in (3), in which it is averaged over x^*, z ($=z^*$), and the three time steps and thus depends on interface-normal distance only. We may therefore also define an interface Kolmogorov length scale η_l^* as η_l evaluated at $y^* = 0$.

Figure 5 shows the variation of η_l with interface-normal distance y^*. It is normalized with the bulk Kolmogorov length scale $\langle\eta\rangle$ in Fig. 5(a) and normalized with the interface Kolmogorov length scale η_l^* in Fig. 5(b). As anticipated from the results of Fig. 3(b), it is immediately obvious that the Kolmogorov length scale increases as it approaches the interface. Recalling that (for our particular Reynolds number and flow configuration) $\delta_\omega \approx \lambda = 1.55h$, it can be seen that this increase of η_l indeed does occur within a region less than or on the order of δ_ω from the interface and hence must be a function of the TNT interface dynamics. While the results of Fig. 5 appear accentuated, a similar finding of η_l increasing as the turbulence boundary is approached was also reported in Ref. [34]. In that case planar turbulent jets were analyzed and the value of η_l was found to increase from the turbulent bulk to the turbulence boundary over a similar distance to that for which there was a jump in the conditional mean vorticity, which is precisely the same finding that we present in this paper. This accentuated effect can be explained by the fact that the flow considered in Ref. [34] (turbulent planar jet) is self-similar, meaning that we would expect only a modest increase in η_l over distances of the order of λ. Nevertheless, the percentage change in η_l over the TNT interface region appears to be comparable to ours. A similar result can also be inferred from the findings in a shear-free TNT interface, produced by means of an oscillating grid, in Ref. [35]. Here $\langle s_{ij}s_{ij}\rangle$ is presented as a function of y^* and it is clearly observed to drop as the turbulence boundary is approached, which corresponds to an increase in η_l.

Further, there appear to be two slopes, perhaps corresponding to the dynamics of the viscous superlayer (larger slope) and the turbulent sublayer (shallower slope) for both the high-speed and

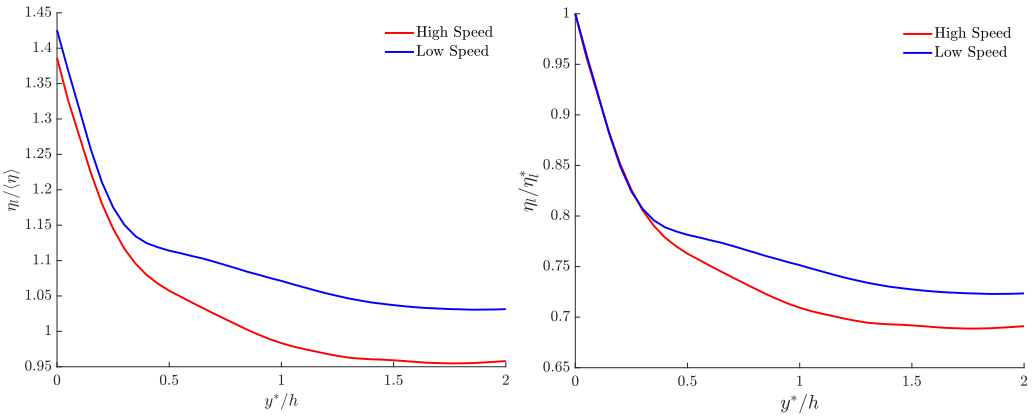

FIG. 5. DNS data set. (a) Variation of the local Kolmogorov length scale η_l with y^* normalized by the bulk mean Kolmogorov length scale $\langle\eta\rangle$ for both interfaces. (b) Variation of the local Kolmogorov length scale with y^* normalized by the value at the interface $\eta_l^* = \eta_l(y^* = 0)$.

the low-speed interfaces. This is evidenced by the fact that the slopes change at the location at which the diffusion term $\mathcal{D}_\omega$ changes from being an enstrophy source term to a sink from Fig. 4, which we used as the definition for the viscous superlayer. Further, the spatial extents of these two slopes also appear to be in roughly the ratio 2:1, which is that observed by Silva *et al.* [13] for the thicknesses of the viscous superlayer (approximately equal to 5η) and the turbulent sublayer (approximately equal to 12η). For $y^* \gtrsim 1.5$, i.e., beyond the TNT interface region and within the turbulent bulk, η_l appears to level off to a constant value. We end this paragraph with a brief note on the physical interpretation of the Kolmogorov length scale within the viscous superlayer. It is the turbulent length scale at which viscosity becomes important but is clearly only meaningful in a turbulent flow and not in a purely viscous (laminar) flow. Figure 4 shows that the inertial vortex stretching term $\mathcal{P}_\omega$ falls to zero at $y^* = 0$ (as expected) but remains comparable in magnitude to $\mathcal{D}_\omega$ until extremely close to the turbulence boundary. In this sense an analogy may be made between the Kolmogorov length scale within the viscous superlayer and the wall unit in wall-bounded turbulence $\delta_\nu = \nu\sqrt{\rho/\tau_w}$, in which τ_w is the time-averaged wall shear stress and ρ is the fluid density. In wall-bounded turbulence this wall unit still collapses the behavior of the buffer layer (in which the viscous and inertial stresses are of comparable magnitude) and the logarithmic layer (negligible viscous stresses) despite being formed from a localized wall statistic.

Figure 5(b) shows that normalization of η_l with the interface Kolmogorov length scale η_l^* collapses the behavior of the high-speed and low-speed interfaces onto the same trend in the very-near-TNT-boundary region, i.e., the presumed viscous superlayer. We point out here that this is a single observation, at one Reynolds number, but this collapse merits further investigation in other flows. Given that viscous processes are significant in this region, this collapse could perhaps be expected when using η_l^* in the same way that δ_ν collapses the turbulence statistics in wall-bounded turbulence. Since inertial processes become increasingly dominant in the turbulent sublayer of the TNT interface, the lack of collapse from $y^*/h \gtrsim 0.5$ onward in Fig. 5(b) suggests that there are fundamental differences in the turbulence structure of the high-speed and low-speed TNT interfaces. This is not surprising when considering the scatter of data observed for the conditional vorticity jumps presented for various turbulent shear flows in the excellent review paper of [3]. In the analogy of wall-bounded turbulence we also observe that the inner viscous scaling does not collapse the outer part of the flow where the influence of viscosity is negligible.

Let us now consider the variation of the local Taylor length scale λ_l in the TNT interface region. The Taylor scale may be defined in many different ways, but we choose a modified version of that

from [36], defined as

$$\lambda^2 = \frac{2u'^2}{\left\langle \left(\frac{\partial u}{\partial x}\right)^2 \right\rangle}. \tag{4}$$

Equation (4) is based upon an assumption of statistically isotropic small-scale turbulence and so noting that $\varepsilon = 15\nu\langle(\partial u/\partial x)^2\rangle$ under an assumption of small-scale isotropy, we arrive at the final formulation for our Taylor length scale

$$\lambda = \left(\frac{30\nu u'^2}{\langle\varepsilon\rangle}\right)^{1/2} = \left(\frac{15u'^2}{\langle s_{ij}s_{ij}\rangle}\right)^{1/2} \tag{5}$$

in which the fully three-dimensional strain-rate tensor is used and no assumptions regarding small-scale isotropy are made. Again we will vary the definition of the ensemble such that we can compute a local Taylor length scale λ_l, which is again a function of y^*. Since there are numerous ways in which to compute the Taylor scale, we also recomputed all of our results in several different ways (including fitting a parabola to the autocorrelation function of the velocity fluctuations) and obtained identical qualitative and extremely similar quantitative results.

Figure 6 shows the variation of λ_l with y^* normalized by the bulk Kolmogorov length scale $\langle\eta\rangle$ in Fig. 6(a) and the local Kolmogorov length scale in Fig. 6(b). We can again see that there is a very significant rise in the ratios of λ_l/η (whether $\eta = \langle\eta\rangle$ or $\eta = \eta_l$) in the very-near-TNT-boundary region, i.e., the presumed viscous superlayer. Figure 6(a) is qualitatively similar to the observations of Ref. [11] that λ_l slightly decreases in the turbulent sublayer before increasing sharply as the turbulence boundary is reached. The behavior that we observe for the variation of both η_l and λ_l with y^* is thus similar to that previously presented in self-similar flows [11,34]. Of most significance, however, is the fact that it is classically assumed that $\lambda/\eta \sim \mathrm{Re}_\lambda^{1/2}$. Figure 6(c) shows the variation of the local Taylor Reynolds number Re_λ versus y^*, which confirms that the qualitative behavior of the ratio λ_l/η is indeed a symptom of the variation of Re_λ across the TNT interface region. However, $(\lambda_l/\eta_l)^2$ clearly does not precisely vary with Re_λ across the TNT interface, as would be required by the $\lambda/\eta \sim \mathrm{Re}_\lambda^{1/2}$ scaling, when comparing the solid and dashed lines of Fig. 6(c). This suggests that there may be at the very least a subtle change in the physics which modifies the (λ_l/η_l) scaling in the TNT interface region. Two possible explanations for this finding are that (i) the local turbulent Reynolds number in the TNT interface region is different from that in the bulk of the flow or (ii) the dynamics of the TNT interface region introduce significant anisotropy that affects the $\lambda/\eta \sim \mathrm{Re}_\lambda^{1/2}$ scaling.

Point (i) is confirmed by Fig. 6(c). As for (ii), the derivation of the scaling $\lambda/\eta \sim \mathrm{Re}_\lambda^{1/2}$ relies on Kolmogorov's first similarity hypothesis [36]. This assumes a universal (and therefore isotropic) form of the fine-scale motions of turbulence with a very large separation in scale space from the (directional) energy-containing motions. We will now explore this small-scale (an)isotropy in Sec. III E.

E. Small-scale anisotropy in the TNT interface region

We will quantify the small-scale anisotropy by using the following ratio Σ, which we define as the anisotropy ratio:

$$\Sigma = \frac{\left\langle \left(\frac{\partial u_{y^*}}{\partial y^*}\right)^2 \right\rangle}{\left\langle \left(\frac{\partial u_{x^*}}{\partial x^*}\right)^2 \right\rangle}. \tag{6}$$

Here the velocity vector has been defined in terms of the interface coordinate system as $\boldsymbol{u} = (u_{x^*}, u_{y^*}, u_z)^T$ (i.e., u_{y^*} is the velocity component normal to the interface) and the differentiation has been performed along the x^* and y^* directions, i.e., tangential and perpendicular to the interface,

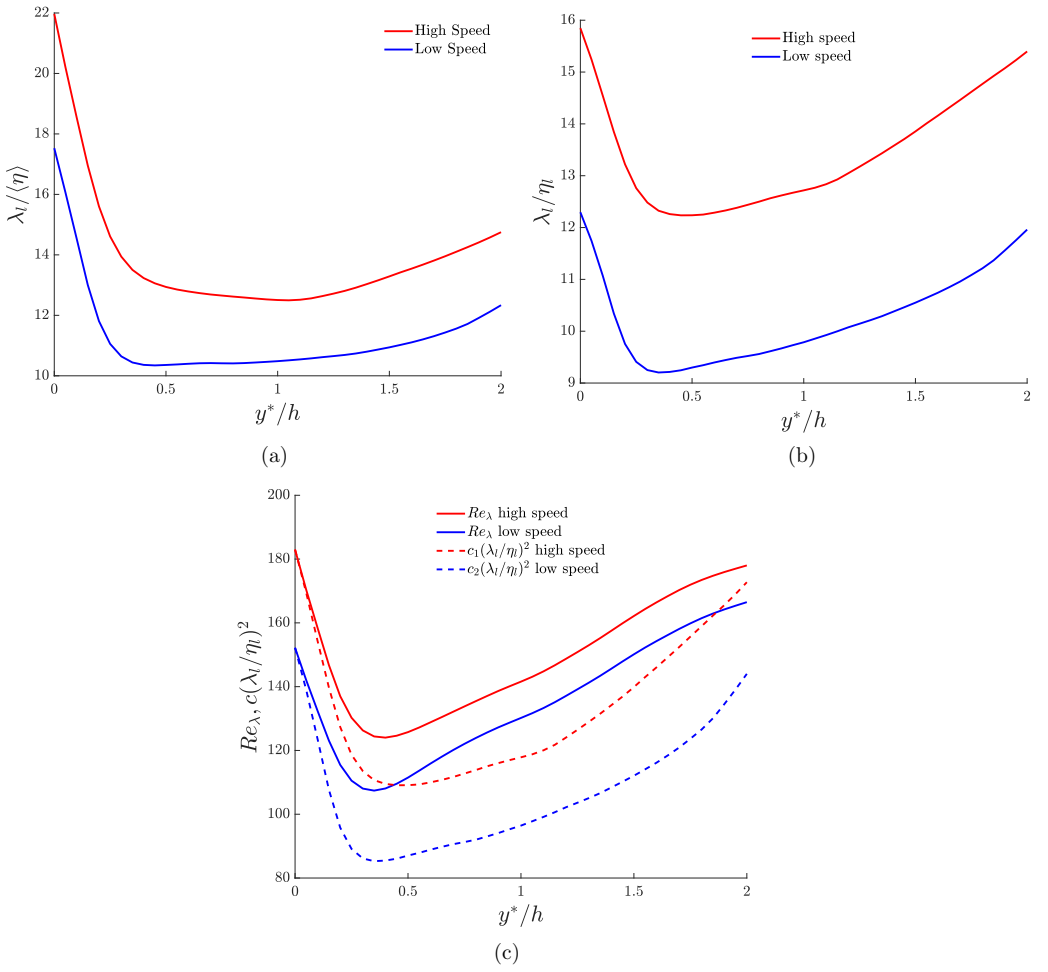

FIG. 6. DNS data set. (a) Variation of local Taylor length scale λ_l with y^* normalized by the bulk mean Kolmogorov length scale $\langle\eta\rangle$ for both interfaces. (b) Variation of the local Taylor length scale with y^* normalized by the local Kolmogorov length scale η_l. (c) Variation of the local Taylor Reynolds number Re_λ with y^* (solid lines) and variation of $(\lambda_l/\eta_l)^2$, multiplied by some constant to match Re_λ at $y^* = 0$, with y^*.

where required. We again perform the ensemble averaging in the x^* and $z^* = z$ directions such that $\Sigma = \Sigma(y^*)$. The ratio Σ is unity for an isotropic flow and so excursions from unity signify small-scale anisotropy.

Figure 7 shows the variation of both Σ and the local Kolmogorov length scale η_l with y^* for the low-speed TNT interface [Fig. 7(a)] and high-speed TNT interface [Fig. 7(b)]. We can see that Σ reaches a maximum within the TNT interface, from values that approach unity in the turbulent bulk. In both cases this region of increased small-scale anisotropy exactly coincides with the rise of η_l. In both the low-speed and high-speed TNT interfaces it can be seen that the maximum value of Σ is reached at precisely the same location at which the slope $d\eta_l/dy^*$ increases sharply, i.e., the presumed boundary between the turbulent sublayer and the viscous superlayer. The small-scale anisotropy is then reduced in the very-near-TNT-boundary region, in the viscous superlayer.

A similar anisotropy was found in the decaying shear-free turbulence results presented in Ref. [37]. By consideration of a mixed physical and spectral space enstrophy budget they were

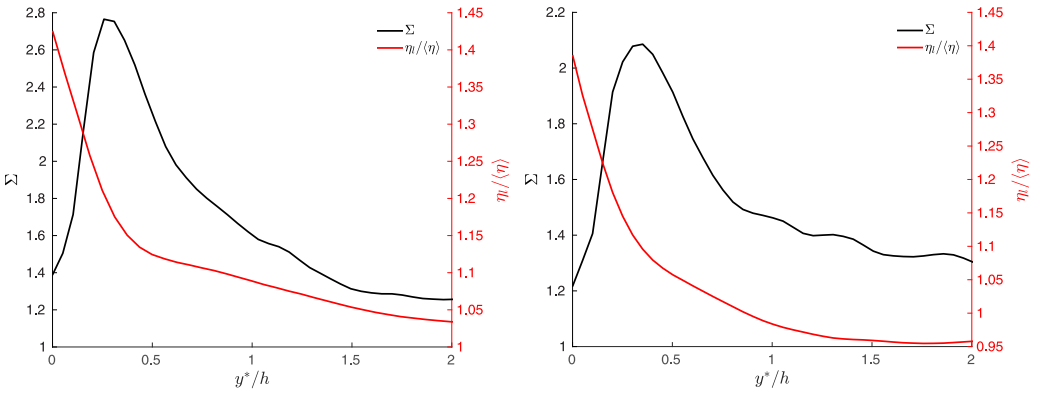

FIG. 7. DNS data set. Anisotropy ratio Σ and local Kolmogorov length scale η_l, normalized by the bulk Kolmogorov length scale $\langle\eta\rangle$ as a function of y^* for (a) the low-speed TNT interface and (b) the high-speed TNT interface.

able to show a substantial degree of anisotropy in the interfacial region of their flow, where the turbulent fluid meets the nonturbulent fluid. In particular, they observed that viscous diffusion occurred at length scales in excess of those responsible for viscous mechanisms, i.e., dissipation, in homogeneous turbulence. They observed that viscous diffusion occurred at large length scales in a direction parallel to the interface, even in the thin viscous superlayer close to their turbulence boundary. This was attributed to an anisotropic enstrophy cascade which produced large structures parallel to the interface, even though the viscous superlayer remained thin (approximately equal to 4η). Such results are clearly consistent with our findings in which the gradients normal to the interface exceed those parallel to the interface.

In order to broaden our discussion of the importance of small-scale anisotropy in the TNT interface region we will now consider the variation of the local Kolmogorov length scale η_l and small-scale anisotropy in the TNT interface regions of a number of turbulent jets. For the experimental data a similar approach to the one described in Sec. III A was used to define the location of the TNT boundary in which a threshold on enstrophy ω^2 was used. Rather than using the interface coordinate system the results are presented simply in terms of the radial distance with respect to the TNT boundary location which was set to $r_i = 0$. This suffices for our purposes since the interface is predominantly in the azimuthal direction, meaning that typically r_i lies close to perpendicular to the interface. The anisotropy measure that we choose to examine is defined as

$$K_2 = 2\frac{\left\langle\left(\frac{\partial u_x}{\partial x}\right)^2\right\rangle}{\left\langle\left(\frac{\partial u_\theta}{\partial x}\right)^2\right\rangle}, \tag{7}$$

in which u_x and u_θ are the streamwise and azimuthal components of velocity, respectively, with x correspondingly the streamwise coordinate. Again, K_2 is equal to unity for an isotropic flow and hence departures from unity are interpreted as an increase in the small-scale anisotropy.

Figure 8 presents the variation of the local Kolmogorov length scale η_l and isotropy measure K_2 as a function of radial distance from the TNT interface r_i for a variety of experimental jet test cases. Note that in the near field of the jet ($x/D = 2$) the small-sale anisotropy in the turbulent bulk is quite significant, whereas K_2 approaches unity (i.e., small-scale isotropy) in the turbulent bulk for $x/D = 25$. We see similar trends as presented in Fig. 7 with an increase in the local Kolmogorov length scale approaching the TNT boundary ($r_i = 0$) occurring concurrently with an increase in the small-scale anisotropy for all jet test cases. Note that the spatial resolution of this tomographic PIV data is insufficient to resolve the viscous superlayer, of presumed thickness approximately equal

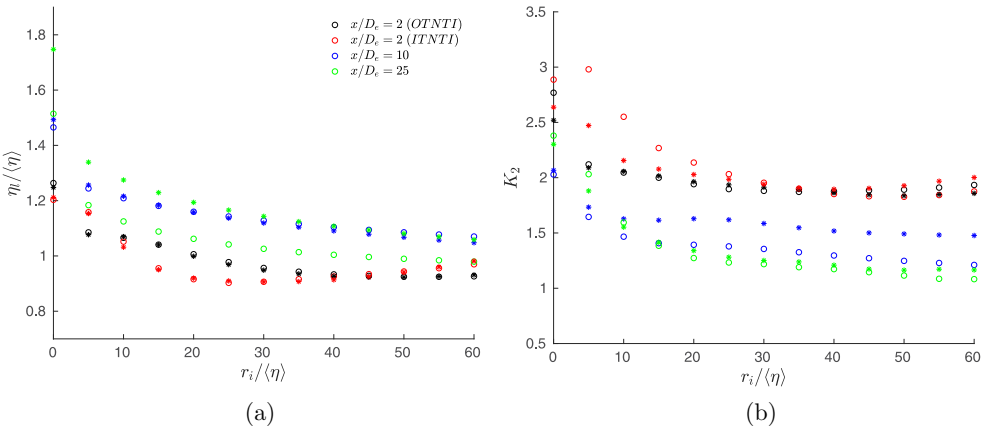

FIG. 8. Tomographic PIV data set. (a) Local Kolmogorov length scale η_l, normalized by the bulk Kolmogorov length scale $\langle\eta\rangle$, and (b) anisotropy ratio K_2 as a function of radial distance r_i from the TNT interface. The $\circ$ denote the round jet and $*$ the fractal jet. Here OTNTI refers to the outer TNT interface and ITNTI refers to the inner TNT interface at the measurement station $x/D = 2$.

to 5η [13], which explains why we do not see the subsequent decrease in K_2 for very small r_i. These trends are observed at all three streamwise locations explored including $x/D = 2$, in which the Kelvin-Helmholtz azimuthal vortices are dominant (for the round jet), and $x/D = 25$, where the turbulence is fully developed and the mean velocity and Reynolds stress profiles have become self-similar (for both jets) [17]. Nevertheless, the small-scale anisotropy and Kolmogorov length scale are always shown to increase as the TNT boundary is approached. This is also observed for the outer TNT interface, i.e., between the jet fluid and the quiescent background fluid, and the inner TNT interface between the turbulent axisymmetric shear layer and the potential core of the jet at $x/D = 2$. These results give us more confidence that the small-scale anisotropy in the TNT interface is an important consideration for a variety of turbulent shear flows.

IV. DISCUSSION AND CONCLUSIONS

In this paper we have considered a number of different TNT interfaces. These include those in a planar turbulent mixing layer for which the turbulent fluid is advecting both more and less rapidly than the nonturbulent fluid. We also considered a series of turbulent jets, with and without the coherent structures being suppressed and both the inner and outer interfaces in the near field, where two TNT interfaces exist. We have shown that the local Kolmogorov length scale η_l increases in size as you approach the TNT boundary, regardless of the type of TNT interface. This is an important consideration when determining the true scaling for δ_ω, the TNT interface thickness, since most often a bulk Kolmogorov (or Taylor) length scale is used rather than the local scaling. We subsequently drew an analogy between a TNT interface and a wall for wall-bounded turbulence. Much like the wall unit $\delta_\nu = \nu\sqrt{\rho/\tau_w}$ in the laminar sublayer of wall-bounded turbulence, it seems that the local Kolmogorov length scale from the TNT boundary itself collapses the variation of η_l with normal distance from the TNT boundary in the viscous superlayer (at least for the mixing-layer flow that we consider). It does not however collapse this variation in the turbulent sublayer where the inertial processes appear to vary from TNT interface to TNT interface, which does not make them amenable to such a viscous scaling.

The wall also introduces anisotropy into a wall-bounded turbulent flow and we additionally show that this is the case with the TNT boundary. The small-scale anisotropy of the flow increases to a maximum at the same interface-normal location as the mean viscous diffusion of enstrophy crosses zero, i.e., the viscous diffusion term $\mathcal{D}_\omega$ transitions from being a source of enstrophy immediately

adjacent to the turbulence boundary to becoming a sink, or negligible, within the turbulent sublayer or turbulent bulk of the flow. This location is also that at which the slopes of the functions of local Kolmogorov and Taylor scales with respect to interface-normal distance y^* change, due to the fact that the dissipation rate no longer increases exponentially with y^*. Combining this information gives a more robust definition for the boundary between the viscous superlayer and the turbulent sublayer, i.e., the y^* location at which $\mathcal{D}_\omega = 0$, which does not depend on some arbitrarily chosen threshold. The marked changes in flow physics at this location perhaps hints at the fact that these two layers are quite distinct from one another. We additionally note that this anisotropic behavior appears to be common across flows with substantially different turbulent structures. This includes both the fractal and round jets (in which the large-scale coherent structures were and were not suppressed, respectively) and the near field and far fields. This suggests that while the flow physics within the TNT interface region must adjust to that in the turbulent bulk there may be a near-interface cycle, analogous to the near-wall cycle of wall-bounded turbulence, governing the flow's behavior within the TNT interface region.

Our analogy between the TNT interface and a wall hinges on the introduction of anisotropy as both are approached and scaling of the very-near-wall/TNT boundary with a (local) viscous length scale. This is of course overly simplistic, not least because a wavy wall is in fact a very poor analogy for a TNT interface and pressure fluctuations can penetrate the TNT interface but not a wall. However, it is reasonably easy for one to picture the TNT boundary as a blockage as far as the turbulent eddies within the TNT interface are concerned, leading to increased velocity gradients in the interface-normal direction, as shown in Fig. 7. The analogy breaks down when considering that the Kolmogorov length scale decreases as one approaches a wall [see, e.g., (8) in Ref. [38]], whereas for a TNT interface we show that it increases

$$\eta \approx \left(\frac{\nu^3 \kappa y}{(\tau_w/\rho)^{3/2}} \right). \tag{8}$$

Nevertheless, we think that this is quite a useful analogy to draw due to the importance that we place on the small-scale anisotropy in the TNT interface which strongly influences the local turbulent length scales.

We show here that in the TNT interface region the small scales are in fact highly anisotropic. We demonstrate this for a variety of spatially developing flows including axisymmetric jets at various streamwise locations and a mixing layer. Additionally, the local turbulent Reynolds number varies significantly throughout the TNT interface region. This variation in local turbulent Reynolds number leads to a variation in the ratio of local turbulent length scales (λ_l/η_l) across the TNT interface region, evident in Fig. 6. The high degree of anisotropy in the TNT interface region is evident in Figs. 7 and 8, and it occurs concurrently with the variation in λ_l/η_l. While the local turbulent Reynolds number and ratio λ_l/η_l vary across the TNT interface region, they do not precisely vary in the fashion $\lambda_l/\eta_l \sim \mathrm{Re}_{\lambda_l}^{1/2}$. A possible explanation for this is the high degree of anisotropy since the derivation of $\lambda/\eta \sim \mathrm{Re}_{\lambda}^{1/2}$ is reliant upon Kolmogorov's first similarity hypothesis. While not wishing to comment on the "correct" scaling for δ_ω, we urge caution in determining the scaling of the TNT interface thickness from simple Reynolds number scaling arguments for flows that are not self-similar, where a single turbulent length scale is inadequate to describe the behavior of the flow across its cross-stream extent. In such flows, including the ones considered in this paper, local turbulent length scales appear to give a better collapse of the data.

ACKNOWLEDGMENT

O.R.H.B. and M.B. would like to acknowledge the financial support given by the Engineering and Physical Sciences Research Council through Grant No. EP/L023520/1.

[1] B. B. Mandelbrot, On the geometry of homogeneous turbulence, with stress on the fractal dimension of the iso-surfaces of scalars, J. Fluid Mech. **72**, 401 (1975).
[2] K. R. Sreenivasan and C. Meneveau, The fractal facets of turbulence, J. Fluid Mech. **173**, 357 (1986).
[3] C. B. da Silva, J. C. R. Hunt, I. Eames, and J. Westerweel, Interfacial layers between regions of different turbulence intensity, Annu. Rev. Fluid Mech. **46**, 567 (2014).
[4] S. Corrsin and A. L. Kistler, Free-stream boundaries of turbulent flows, NACA Report No. TN-1244, (1955), https://ntrs.nasa.gov/search.jsp?R=19930092246.
[5] M. Holzner and B. Lüthi, Laminar Superlayer at the Turbulence Boundary, Phys. Rev. Lett. **106**, 134503 (2011).
[6] R. R. Taveira and C. B. da Silva, Characteristics of the viscous superlayer in shear free turbulence and in planar turbulent jets, Phys. Fluids **26**, 021702 (2014).
[7] C. B. da Silva and R. R. Taveira, The thickness of the turbulent/nonturbulent interface is equal to the radius of the large vorticity structures near the edge of the shear layer, Phys. Fluids **22**, 121702 (2010).
[8] M. van Reeuwijk and M. Holzner, The turbulence boundary of a temporal jet, J. Fluid Mech. **739**, 254 (2014).
[9] D. K. Bisset, J. C. R. Hunt, and M. M. Rogers, The turbulent/non-turbulent interface bounding a far wake, J. Fluid Mech. **451**, 383 (2002).
[10] J. Westerweel, C. Fukushima, J. M. Pedersen, and J. C. R. Hunt, Momentum and scalar transport at the turbulent/non-turbulent interface of a jet, J. Fluid Mech. **631**, 199 (2009).
[11] A. Attili, J. C. Cristancho, and F. Bisetti, Statistics of the turbulent/non-turbulent interface in a spatially developing mixing layer, J. Turbul. **15**, 555 (2014).
[12] K. Chauhan, J. Philip, C. M. de Silva, N. Hutchins, and I. Marusic, The turbulent/non-turbulent interface and entrainment in a boundary layer, J. Fluid Mech. **742**, 119 (2014).
[13] T. S. Silva, M. Zecchetto, and C. B. da Silva, The scaling of the turbulent/non-turbulent interface at high Reynolds numbers, J. Fluid Mech. **843**, 156 (2018).
[14] T. Watanabe, Y. Sakai, K. Nagata, Y. Ito, and T. Hayase, Vortex stretching and compression near the turbulent/non-turbulent interface in a planar jet, J. Fluid Mech. **758**, 754 (2014).
[15] T. Watanabe, Y. Sakai, K. Nagata, Y. Ito, and T. Hayase, Turbulent mixing of passive scalar near turbulent and non-turbulent interface in mixing layers, Phys. Fluids **27**, 085109 (2015).
[16] T. Watanabe, C. B. da Silva, Y. Sakai, K. Nagata, and T. Hayase, Lagrangian properties of the entrainment across turbulent/non-turbulent interface layers, Phys. Fluids **28**, 031701 (2016).
[17] M. Breda and O. R. H. Buxton, Influence of coherent structures on the evolution of an axisymmetric turbulent jet, Phys. Fluids **30**, 035109 (2018).
[18] O. R. H. Buxton, S. Laizet, and B. Ganapathisubramani, The interaction between strain-rate and rotation in shear flow turbulence from inertial range to dissipative length scales, Phys. Fluids **23**, 061704 (2011).
[19] S. Laizet, S. Lardeau, and E. Lamballais, Direct numerical simulation of a mixing layer downstream a thick splitter plate, Phys. Fluids **22**, 015104 (2010).
[20] O. R. H. Buxton, Modulation of the velocity gradient tensor by concurrent large-scale velocity fluctuations in a turbulent mixing layer, J. Fluid Mech. **777**, R1 (2015).
[21] P. K. Rabey, A. Wynn, and O. R. H. Buxton, The kinematics of the reduced velocity gradient tensor in a fully developed turbulent free shear flow, J. Fluid Mech. **767**, 627 (2015).
[22] S. Laizet and E. Lamballais, High-order compact schemes for incompressible flows: A simple and efficient method with quasi-spectral accuracy, J. Comput. Phys. **228**, 5989 (2009).
[23] M. Breda and O. R. H. Buxton, Effects of multiscale geometry on the large-scale coherent structures of an axisymmetric turbulent jet, J. Visual. **21**, 525 (2018).
[24] J. Nedić, J. C. Vassilicos, and B. Ganapathisubramani, Axisymmetric Turbulent Wakes with New Nonequilibrium Similarity Scalings, Phys. Rev. Lett. **111**, 144503 (2013).
[25] G. E. Elsinga, F. Scarano, B. Wieneke, and B. W. van Oudheusden, Tomographic particle image velocimetry, Exp. Fluids **41**, 933 (2006).
[26] G. T. Herman and A. Lent, Iterative reconstruction algorithms, Comput. Biol. Med. **6**, 273 (1976).
[27] B. Wieneke, Volume self-calibration for 3D particle image velocimetry, Exp. Fluids **45**, 549 (2008).

[28] M. Novara, K. J. Batenburg, and F. Scarano, Motion tracking-enhanced MART for tomographic PIV, Meas. Sci. Technol. **21**, 035401 (2010).
[29] C. M. de Silva, J. Philip, and I. Marusic, Minimization of divergence error in volumetric velocity measurements and implications for turbulence statistics, Exp. Fluids **54**, 1557 (2013).
[30] G. Borrell and J. Jiménez, Properties of the turbulent/non-turbulent interface in boundary layers, J. Fluid Mech. **801**, 554 (2016).
[31] D. Mistry, J. Philip, J. R. Dawson, and I. Marusic, Entrainment at multi-scales across the turbulent/non-turbulent interface in an axisymmetric jet, J. Fluid Mech. **802**, 690 (2016).
[32] G. I. Taylor, Production and dissipation of vorticity in a turbulent fluid, Proc. R. Soc. London Ser. A **164**, 15 (1938).
[33] C. B. da Silva and J. C. F. Pereira, Invariants of the velocity-gradient, rate-of-strain, and rate-of-rotation tensors across the turbulent/nonturbulent interface in jets, Phys. Fluids **20**, 055101 (2008).
[34] R. R. Taveira and C. B. da Silva, Kinetic energy budgets near the turbulent/nonturbulent interface in jets, Phys. Fluids **25**, 015114 (2013).
[35] M. Holzner, A. Liberzon, N. Nikitin, W. Kinzelbach, and A. Tsinober, Small-scale aspects of flows in proximity of the turbulent/nonturbulent interface, Phys. Fluids **19**, 071702 (2007).
[36] S. B. Pope, *Turbulent Flows* (Cambridge University Press, Cambridge, 2000).
[37] A. Cimarelli, G. Cocconi, B. Frohnapfel, and E. De Angelis, Spectral enstrophy budget in a shear-less flow with turbulent/non-turbulent interface, Phys. Fluids **27**, 125106 (2015).
[38] T.-H. Shih and J. L. Lumley, Kolmogorov behaviour of near-wall turbulence and its application in turbulence modelling, Int. J. Comput. Fluid Dyn. **1**, 43 (1993).